ELSEVIER

Polymer 40 (1999) 5023–5033

polymer

Dielectric on-line spectroscopy during extrusion of polymer blends

Arjen Boersma*, Jan van Turnhout

Delft University of Technology, Faculty of Applied Science, Department of Polymer Technology, Julianalaan 136, 2628 BL Delft, The Netherlands

Received 29 June 1998; received in revised form 17 September 1998; accepted 9 October 1998

Abstract

Dielectric spectroscopy is a technique which is still hardly used for on-line characterization of polymers. In this article we describe its use at medium frequencies (between 10 Hz and 1 MHz) for on-line monitoring of the morphology of polymer blends during extrusion. A sheet extrusion die containing two electrodes, made it possible to perform the dielectric on-line analysis.

A blend of a thermotropic Liquid Crystalline Polymer (LCP) dispersed in polypropylene was used to follow the change in shape and co-continuity of the LCP phase with increasing extrusion speed. The creation of a more fibrous structure at higher shear rates was demonstrated by the dielectric technique as well as by SEM analysis.

A blend of a thermotropic liquid crystalline polymer dispersed in polystyrene was chosen to study the evolution of the size of the LCP inclusions with increasing extruder speed. The Böttcher–Trukhan relation enabled us to convert the dielectric data to values of the particle size and a decrease in size with increasing shear rate was found. This was confirmed by SEM micrographs.

The experiments and analysis presented in this article show that dielectric spectroscopy proves to be a valuable tool for on-line characterization of the microstructure of polymer blends. © 1999 Elsevier Science Ltd. All rights reserved.

Keywords: Dielectric spectroscopy; On-line characterization; Morphology

1. Introduction

The on-line characterization and analysis of product flows in the polymer industry receives more and more attention for further improvement of product quality and economical profits [1]. The on-line technique most frequently used, is infrared spectroscopy, which for instance is applied for the determination of the composition of polymer blends and solutions, reaction monitoring and surface characterization [2].

A second technique is the on-line monitoring of the rheological properties of a product in an extruder or a reactor to ensure product quality. The two most common rheometers are the bypass and the return stream type. In the bypass rheometer the polymer is extruded into the open and is lost, whereas the return stream rheometer puts the extruded polymer back into the process [3]. On-line rheometers can be applied to determine the viscosity over a broad shear rate range [4–6], or just the melt flow index.

Optical methods such as microscopy and light scattering are used for the evaluation of morphologies in immiscible polymer blends [7,8]. Particle shape, size and orientation can be assessed with these techniques. A disadvantage of the optical techniques, including IR spectroscopy, is the necessity for the polymer flow to be transparent for the light used. On-line ultrasonic methods are used for the determination of changes in pressure, temperature, specific volume and flow behaviour in polymer melts [9].

Occasionally, on-line NMR measurements have been applied for crystallinity, density (of PE), tacticity (of PP) and viscosity/melt index/molecular weight measurements [10]. NMR is also suitable for the measurement of the composition of co-polymer/polymer blends. X-ray diffraction has been explored for on-line monitoring of structural changes (crystallinity and orientation) during processing of nylon fibres [11]. The disadvantages of the latter two techniques are the size and costs of the equipment involved.

A technique which, so far, has been scarcely exploited for on-line product control is dielectric spectroscopy. Although the frequency range over which dielectric spectroscopy can be applied is very broad (1 MHz–40 GHz), present on-line applications only cover the microwave regime of the spectrum. The reason for this is twofold. Most of the substances monitored contain water. At low frequency this causes interfacial and/or electrode polarization, which obscures the molecular dipole relaxations. This problem was circumvented recently for biomass measurements by using inductive dielectric spectroscopy in which no electrodes are used [12]. A second reason is the speed of data acquisition, which

* Corresponding author.
E-mail address: turnhout@stm.tudelft.nl (J. van Turnhout)

0032-3861/99/$ - see front matter © 1999 Elsevier Science Ltd. All rights reserved.
PII: S0032-3861(98)00744-7

is higher for higher frequencies. However, the equipment, the data acquisition and data analysis of microwave measurements are more complicated than those of low and medium frequency measurements.

For microwave measurements on liquid flows, two different kinds of on-line measurement setups have been proposed. An open-ended coaxial probe has been applied for dielectric measurements on saline solutions as a function of the salt content [13]. A second setup is the microwave transmission technique, which has been used for the analysis of oil-in-water and water-in-oil emulsions [14]. It is possible to determine the emulsion type (o/w or w/o) and the water content of the emulsion. Admittedly, both measurement techniques are important for the oil industry. In the food industry microwave spectroscopy is used to measure the moisture content in various organic products [15,16].

To our knowledge on-line dielectric/microwave spectroscopy has been scarcely exploited in the polymer industry. A few patents are known [17–19] in which dielectric spectroscopy is used for composition and viscosity measurements. In this article we will assess the possibilities of dielectric spectroscopy at medium frequencies (10 Hz–1 MHz) for on-line monitoring the morphology of polymer blends during extrusion. We have shown in two previous articles [20,21] that dielectric spectroscopy can be applied to follow in real time morphology changes during the breakup of polymer fibres in a polymer matrix. It was possible to convert the measured dielectric response into predictions about the actual shape of the inclusions in the blend. We will now extend this knowledge of off-line spectroscopy to a useful measurement strategy for on-line experiments.

The influence of the particle size on the dielectric response of polymer blends was discussed in a third article [22]. It turned out that if the size of the inclusions is of the same order of magnitude as the Debye screening length inside the particles, the dielectric response (relaxation strength/relaxation time) deviates from the ''ideal'' case predicted by the conventional mixture theories.

In this article we will indicate how the particle size and shape during extrusion of a blend of a thermotropic liquid crystalline polymer (TLCP) and various thermoplastic polymers can be ascertained. These so called self-reinforcing blends have the ability to form fibrous structures during processing. We have used an extruder in combination with static mixture elements to ensure the formation of the desired morphology. An alternative method of processing self-reinforcing blends was proposed by Roetting et al. [23,24]. After grinding both matrix polymer and TLCP, a powder-fibre mixture was formed. This mixture was extruded through a wire cloth and die using a piston so that a more homogeneously reinforced blend was obtained.

The use of dielectric spectroscopy has several advantages for the on-line characterization of polymer flows. The first advantage is the absence of the necessity for the polymer melt to be transparent (in contrast to IR and optical techniques). A second advantage is the relative simple and compact equipment compared to e.g. NMR and X-ray. The permittivity is an average over the total volume between the electrodes, whereas the IR, optical and X-ray techniques only sample a small fraction of the total volume. Furthermore, dielectric spectroscopy is a relatively fast technique. There is no need for an exposure time, the number of frequencies used is the only limiting factor for the sampling speed. The data can be automatically analyzed and easily converted to values of composition, particle shape and even particle size.

In order to perform on-line dielectric experiments during extrusion of polymer blends, we have constructed a special sheet extrusion die. Two plane-parallel electrodes were implemented in the die, between which the molten polymer flowed. In this article we will explore the use of dielectric spectroscopy in order to obtain information about the most relevant parameters during extrusion: viz. the volume fraction of dispersed phase, the distribution of this phase over the blend and the shape and size of the inclusions in the blend.

2. Theory

2.1. Generalized Böttcher–Trukhan mixture theory

We have previously shown [20,21] that the mixture formula derived by Böttcher, Polder and Hsu can describe the dielectric response of a Vectra B950-polypropylene blend at low concentrations (0–15 vol.%) quite well. As in this article we will perform experiments on the same system, the Böttcher–Hsu equation has again been chosen for the data processing. Trukhan first discussed the influence of the particle size on the dielectric response [25,26] in a system of partially conducting spheres in an insulating matrix, by taking diffusion into account. Malmgren-Hansen [27] extended this approach to higher volume fractions and incorporated the particle size in the Bruggeman theory and derived the Bruggeman–Trukhan equation.

We combined the Trukhan approach with the Böttcher equation and derived the Böttcher–Trukhan mixture relation for conducting particles in an isolating matrix [22]. This equation describes the interfacial polarization caused by the difference in conductivity between the matrix and the dispersed phase and incorporates the diffusion of the charge carriers (ions). A complex size factor β^* was introduced to account for the size of the inclusions. The Böttcher–Trukhan equation derived in the previous article [22] can be extended to include the shape of the particles (Appendix A). We thus obtain the generalized Böttcher–Trukhan equation:

$$\varepsilon^* = \varepsilon_1 + \varepsilon^*\phi_2 \frac{\varepsilon_2 - \varepsilon_1(1-\beta^*)}{\varepsilon_2 A_k + \varepsilon^*(1-A_k)(1-\beta^*)} \tag{1}$$

ε^* is the complex permittivity of the blend and ε_1 and ε_2 are the real parts of the permittivity of the matrix and the

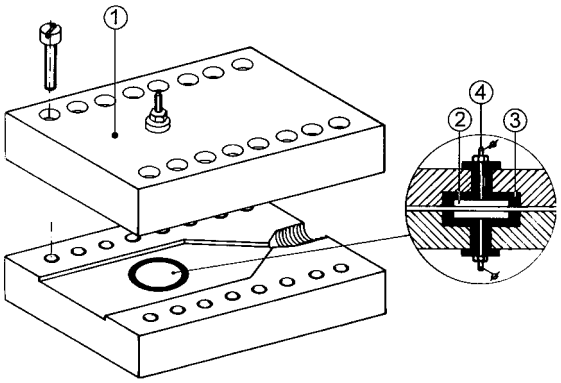

Fig. 1. Schematic representation of the sheet extrusion die for dielectric experiments during the extrusion of polymer blends. The inset shows an enlargement of the parallel plate electrodes built in.

dispersed phase respectively. ϕ_2 is the volume fraction of dispersed phase. Obviously, the two most important parameters in Eq. (1) are the shape factor, A_k, and the size factor, β^*, of the inclusions. Therefore, we rewrite Eq. (1) into:

$$\frac{A_k}{\varepsilon^*} = \frac{\phi_1}{\varepsilon^* - \varepsilon_2/(1-\beta^*)} + \frac{\phi_2}{\varepsilon^* - \varepsilon_1} \qquad (1')$$

Both parameters are needed to characterize the morphology of the blend. A_k is the parameter which describes the shape of the dispersed phase and is 1/3 for spheres, 1/2 for fibres and 1 for laminates. β^* is a measure for the size of the dispersed phase. In fact $1/(1-\beta^*)$ acts as a scaling factor to the permittivity of the phase that contains the ions, viz ε_2. The real part of β^* is 1 for very large particles ($r\kappa \gg 1$) and 0 for very small particles ($r\kappa \ll 1$). Furthermore it depends on the shape of the dispersed phase. For spherical inclusions it becomes:

$$\beta_s^*(\omega) = \frac{\kappa^2}{\gamma^{*2}}\left[\frac{[3+(\gamma^* r)^2]\tanh(\gamma^* r) - 3\gamma^* r}{[2+(\gamma^* r)^2]\tanh(\gamma^* r) - 2\gamma^* r}\right] \qquad (2)$$

and for laminates:

$$\beta_l^*(\omega) = \frac{\kappa^2}{\gamma^{*2}}\left[1 - \frac{\tanh(\gamma^* a)}{\gamma^* a}\right] \qquad (3)$$

in which r is the radius of the spherical particles and a half the thickness of the conducting layer. The parameter κ is the inverse Debye length. With ω being the angular frequency, τ_2 the relaxation time of the conduction in the conductive phase and i the imaginary number, $\sqrt{-1}$, the values of the complex parameter γ^* and κ are related by:

$$\gamma^{*2} = \kappa^2(1 + i\omega\tau_2) \qquad (4)$$

By model calculations one can show that the values of β_s^* and β_1^* behave similarly versus both the frequency and the radius, r, or thickness, a, of the dispersed phase. As in this article, we will deal with particle-matrix systems, we will use Eq. (2) to convert the measured β^* to values of the particle size. Note that for $\omega \to 0$, $\gamma \approx \kappa$, and $\beta^*(\omega) = \beta_0'$ while $\beta_0'' = 0$.

2.2. Data processing

For the processing of the dielectric data, we will use merely the high and low frequency limit of Eq. (1). At low frequencies ($\omega \to 0$; 256 Hz in the experiments, for which $\omega\tau_2 \ll 1$) the value of the real part of β^* becomes equal to β_0'. If this value becomes 1 (very large particles), Eq. (1) reduces to the original Böttcher–Hsu equation; as a result the strongest interfacial polarization is reached. At high frequencies ($\omega \to \infty$; 66 kHz in the experiments), β_∞' becomes 0.

Knowing the volume fraction, we should be able to obtain A_k from the high frequency limit ($\beta_\infty' = 0$) and in addition β_0' from the low frequency limit. However, because of uncertainties in the measurements and the approximations made in the theoretical derivations, only either the size (β'_0) or the shape (A_k) parameter has been calculated at the same time and not both. The choice of the parameter to be calculated depends on the morphology derived from the SEM analysis.

We have used the software Maple V R4 from Waterloo Maple Software in the calculations. This makes it possible to calculate the various parameters from the measurements, without having explicit functions for these parameters at hand.

3. Experiments

3.1. Sheet extrusion die

In previous articles [20–22] we have performed dielectric experiments on polymer blends inside a dielectric sample holder. This showed that is was possible to obtain information about the shape and size of the inclusions. The next objective was to perform dielectric on-line measurements on flowing polymer blends. Therefore, we had to construct a new test rig. The easiest way to accomplish this is to insert a parallel plate capacitor inside a sheet extrusion die. A schematic drawing of the die is shown in Fig. 1. Two steel plates of 28 × 140 × 180 mm each {1} are mounted together with bolts. In one of the plates a 0.5 mm deep slit is made. In the middle of the slit two brass electrodes {2} are built in. The diameter of the electrodes is 30 mm and their thickness is 5 mm. They are embedded in a Macor (sintered glass) cup {3} of 40 mm diameter and 10 mm thickness to insulate the electrodes. The electrodes are kept in place with a 4 mm thick brass rod {4}, also insulated by a Macor tube. Co-axial cables connect the brass rods to the dielectric equipment. The sheet extrusion die was heated by means of a heating band {5}. The temperature of the die was kept at 280°C.

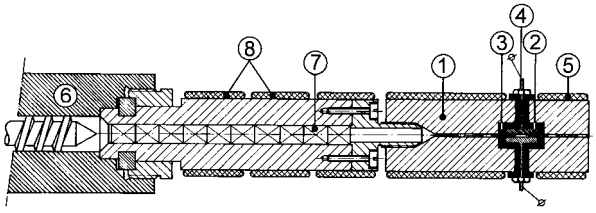

Fig. 2. Schematic representation of the extruder, mixing section and sheet extrusion die used for processing the polymer blends.

3.2. Extruder

The sheet extrusion die is mounted at the exit of a Collin single screw extruder ($D = 20$ mm, $L/D = 20$ {6}). A mixing section between the extruder and the die, containing ten Ross static mixing elements {7}, ensured the formation of the desired morphology. A schematic drawing of the setup is given in Fig. 2. The pellets of the blend polymers were mixed beforehand and fed into the hopper of the extruder. The extruder screw was heated using heating bands with set points: 140, 240 and 300°C. The heating bands of the mixing section {8} were kept at 290°C.

3.3. Dielectric equipment

A Hewlett-Packard 4284A precision LCR-meter was used at frequencies between 32 Hz and 500 kHz. An AC voltage of 1 V was applied between the electrodes. The sheet extrusion die was connected to the ground of the LCR-meter. A number of experiments were performed using the whole frequency range between 32 Hz and 500 kHz, with an average of 5 scans per experiment. The disadvantage of this method is the time necessary for one scan. In order to follow the dielectric properties of the blend more closely while extruding, only two frequencies were used, i.e. 256 Hz and 66 kHz, with 25 scans per experiment. As will be shown later these frequencies are above and below the step in the interfacial relaxation (see Fig. 6).

3.4. Materials

The blends studied consisted of a thermotropic liquid crystalline polymer dispersed in a thermoplastic polymer matrix. The TLCP was the random copolyesteramide Vectra B950 consisting of 60% 2,6-hydroxynaphthoic acid, 20% terephthalic acid and 20% aminophenol, supplied by Hoechst-Celanese (VB). The as-received granules were dried at 180°C for 4 h in a nitrogen atmosphere and kept under vacuum at 60°C afterwards. DSC showed that the melting point of the granules was about 284°C. The thermoplastic polymers were two polypropylene grades: Stamylan P13E10 supplied by DSM (P13) and PLZ 746 from Shell (PLZ), and two polystyrene grades: PS N2000 (PS2) and PS N5000 (PS5) also from Shell.

Three different blends were made at 280°C containing 5, 10 and 20 vol.% Vectra B950. The pellets were mixed in the hopper of the extruder. For the calculation of the weight fractions of the pellets we used the following densities: Vectra B950. 1.36 (RT) and 1.34 g/ml (280°C); polypropylene, 0.91 and 0.72 g/ml; polystyrene, 1.07 and 0.92 g/ml.

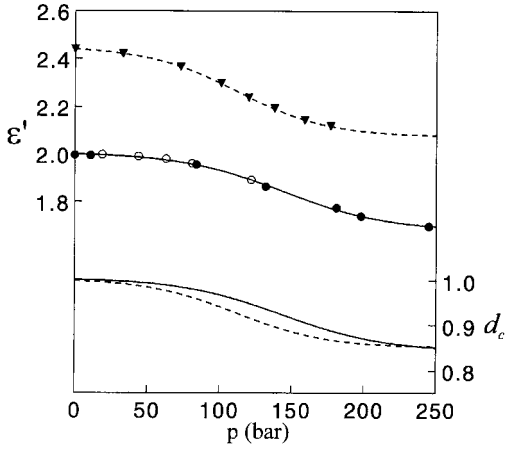

Fig. 3. Measured real permittivity and correction factor, d_c, versus the pressure inside the mixing section of the extruder for three matrix polymers: Polypropylene P13E10 (–●–) and PLZ 746 (–○–); polystyrene N5000 (- -▼- -).

3.5. Rheological characterization

In order to envisage the morphologies formed inside the extruder, the rheological behaviour of the polymers is needed. Rheological experiments were made on the pure polymers under nitrogen using a Rheometrics RMS-800 equipped with a plate and plate geometry (25 mm diameter, 1–2 mm gap). Circular samples were made by compression moulding of granules of polypropylene (P13 and PLZ), polystyrene (PS2 and PS5) and Vectra B950. The viscosity versus shear rate was measured for the matrix polymers at 290°C and for Vectra at 300°C.

3.6. Experimental considerations

During the measurements it turned out that the distance between the two electrodes changed after switching on the extruder, since the pressure built up inside the mixing elements and sheet die was rather large. Although the die was made of steel, the stiffness was insufficient and the electrode spacing became larger. Fig. 3 shows the real part of the permittivity at 125 kHz versus the pressure (measured between the extruder and the mixing section) for the various matrix polymers used.

It turned out that the effect of the pressure on the dielectric data was reversible. This made it possible to correct the measured values of the permittivity for the increased electrode spacing, under the assumption that the blend behaves similar as the pure matrix polymer. As the measured capacitance depends on the pressure (p, bar) inside the die, a correction factor was introduced, $d_c = \varepsilon'_{p\ \mathrm{bar}}/\varepsilon'_{0\ \mathrm{bar}}$, which accounts for the increase in electrode spacing. This value

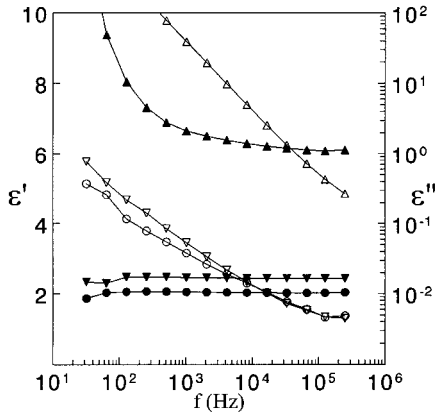

Fig. 4. Permittivity and loss of polypropylene P13E10 ($\varepsilon' = \bullet$, $\varepsilon'' = \circ$), polystyrene N5000 ($\varepsilon'' = \blacktriangledown$, $\varepsilon'' = \triangledown$) and Vectra B950 ($\varepsilon'' = \blacktriangledown$, $\varepsilon'' = \triangledown$) versus frequency.

of d_c is also plotted in Fig. 3. There is only a small difference between the correction parameters of the two polymers studied. Now, we can make a distinction between the genuine and measured (subscript m) values of the real permittivity of the blends:

$$\varepsilon'_m = \varepsilon' d_c \tag{5}$$

The correction factor d_c obtained from Fig. 3 will be used in the calculations. Introducing the low ($\beta_0{}'$) and high ($\beta'_\infty = 0$) frequency values of the real part of the permittivity in Eq. (1) or (1′), we obtain two equations from which the two remaining unknown parameters can be calculated: ϕ_2 and $\beta_0{}'$ or ϕ_2 and A_k. A second approach which does not require knowledge of d_c and uses the measured dielectric loss together will Eq. (1) to obtain three unknown parameters, viz. ϕ_2, d_c and $\beta_0{}'$ or A_k will be discussed in Appendix B.

3.7. Scanning electron microscopy

The morphology (shape and sizes of the particles) of the blends was analyzed using a Philips XL 20 Scanning Electron Microscope (SEM). The samples were cryogenically fractured and sputtered with gold. An accelerating voltage of 15 kV was used.

4. Results and discussions

4.1. Material properties

In order to perform the calculations on the dielectric data of the blends, we must know the properties of the pure polymers. Fig. 4 shows the dielectric data of the high viscous polymers P13 and PS5 and Vectra B950, measured between the electrodes in the sheet die. The low viscous polymers (PLZ and PS2) show similar results. The values of the permittivity of the pure components at 280°C needed for the data processing are listed in Table 1. The temperature 280°C is chosen, because the die in which the dielectric measurements are conducted is kept at this temperature.

The morphologies formed inside the extruder are strongly governed by the rheological properties of the polymers involved. Rheological measurements on the matrix polymers were conducted at 290°C, because this is the temperature of the mixing section. For Vectra B950 this temperature was 300°C, because the last section of the extruder was 300°C and Vectra B950 can be supercooled. The viscosity versus shear rate of all the materials is given in Fig. 5. In Table 1, the viscosities of the polymers at a shear rate of 10 s^{-1} are listed.

Another parameter which has a significant influence on the morphology of the blends is the shear rate inside the extruder. Therefore we have to convert the measured volume flow of the blend to the average shear rate. The easiest way to do this is for Newtonian fluids. Although the viscosity of polymers often follows a power law, we will nonetheless use the Newtonian approach, because we only want an indication of the shear rate. The highest shear rate inside a capillary is located at the wall: $\dot{\gamma}_w = 4Q/(\pi R_c^3)$. Q is the volume flow of the polymer (m^3/s) and R_c the radius of the capillary of the mixing elements (m). The average shear rate inside a capillary becomes: $\langle\dot{\gamma}\rangle = 2/3\dot{\gamma}_w(s^{-1})$.

4.2. Cessation of flow

As the electrode spacing has a marked influence on the uncorrected results of the dielectric experiments during polymer flow, we will start presenting some data after

Table 1
Dielectrical and rheological properties of the pure polymers

Polymer	Code	Dielectrical[a]			Rheological[b]
		ε' (66 kHz)	ε' (256 kHz)	$\beta''_\infty = \varepsilon''/\varepsilon'$ (66 kHz)	η(Pas) ($\dot{\gamma} = 10\ s^{-1}$)
PP P13E10	P13	2.052	2.070	—	1500
PP PLZ746	PLZ	2.052	2.070	—	257
PS N5000	PS5	2.441	2.494	—	337
PS N2000	PS2	2.441	2.494	—	55
Vectra B950	VB	6.101	7.333	0.150	118

[a] The permittivities were measured at 280°C.
[b] The viscosities for the matrix polymers PP and PS were measured at 290°C and for Vectra B950 at 300°C.

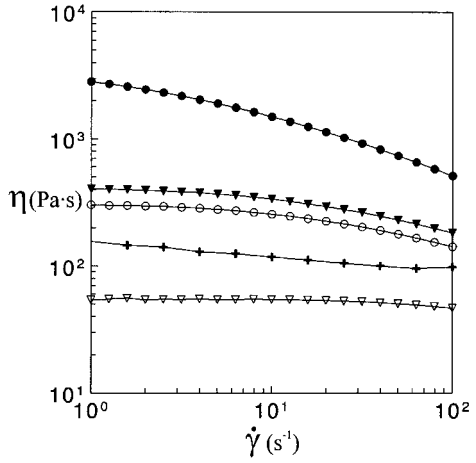

Fig. 5. Viscosity of P13E10 (●), PLZ 746 (○), PS N5000 (▼), PS N2000 (▽) at 290°C and Vectra B950 (+) at 300°C versus shear rate.

cessation of the polymer flow. After extrusion of the blends the extruder is shut down and the polymer is left to relax. This causes the electrodes to assume their equilibrium position and the absolute permittivity can be obtained without correction for the thickness. This means d_c is equal to 1.

4.3. Volume fraction

The first analysis was focused on the volume fraction in the PS5/VB blends. It is clear from Fig. 6 that the relaxation strength of the interfacial polarization increases significantly with increasing volume fraction Vectra. SEM analysis showed that the particles in the blend are relaxed to spheres ($A_k \approx 1/3$) after cessation of the flow. We calculated from the high frequency limit of Eq. (1) the volume fractions and found 5.1, 10.5 and 20.2%. These values are almost equal to the composition of the pellets in the hopper. This means that the high frequency limit of the real permittivity gives a good assessment of the volume fraction.

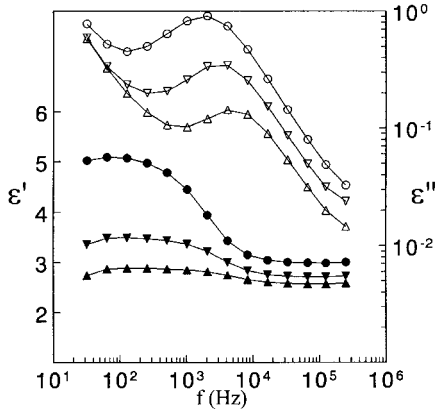

Fig. 6. Permittivity and loss of three Vectra B950-PS N5000 blends: 5 vol.% ($\varepsilon' = \blacktriangle$;, $\varepsilon'' = \triangle$), 10 vol.% ($\varepsilon' = \blacktriangledown$, $\varepsilon'' = \triangledown$) and 20 vol.% ($\varepsilon' = \bullet$, $\varepsilon'' = \circ$) versus frequency.

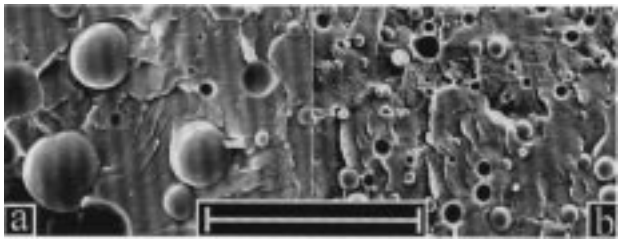

Fig. 7. SEM micrographs of two 10 vol.% Vectra B950-PS blends after relaxation of the morphology: PS N2000 (a, $\beta_0' = 0.98$) and PS N5000 (b, $\beta_0' = 0.91$). The length of the bar is 100 μm.

4.4. Particle size

From the relaxation strength of the samples in Fig. 6 (low frequency limit of Eq. (1)) the value of the value of the shape factor β_0' was obtained. As it is not known yet to what volume fraction the generalized Böttcher–Trukhan equation remains valid, it is difficult to compare the values of β_0' at different volume fractions. Therefore we also calculated β_0' for the PS2/VB blends. When comparing the 10% Vectra blends of both polystyrenes, we find β_0' (PS5/VB) = 0.91 ($r\kappa \approx 12$) and β_0' (PS2/VB) = 0.98 ($r\kappa \approx 50$). This indicates that the size of the particles in the low viscous matrix (PS2) is higher than in the high viscous matrix (PS5). The SEM micrographs in Fig. 7 confirm these conclusions. The average particle radius for PS2 is about 20 μm and for PS5 about 6 μm. This leads to a value of the Debye length ($1/\kappa$) of approximately 0.5 μm. This value was also found in the previous article [22] for a similar system. Corresponding results were obtained for the 5 and 20% blends.

4.5. Breakup of morphology

During extrusion of a blend, a more or less steady state morphology will develop. This morphology will depend on various parameters such as volume fraction, number of mixing elements in the extruder and extrusion speed. After the polymer flow is stopped the morphology will relax to a more stable one. Fibres may breakup or retract. We have compared this relaxation behaviour in two blends: 20 vol % Vectra B950 in a high (P13) and low (PLZ) viscous polypropylene matrix. The flow through the static mixing elements was approximately 17 ml/min, which introduces an average shear rate of the polymer of about 25 s^{-1}. At time zero the extruder was shut down and a number of frequency scans was taken. Fig. 8(a) shows the results of the P13/VB flow and Fig. 8(b) that of PLZ/VB. Both graphs are corrected for the change in electrode spacing using Fig. 3 and Eq. (5).

The first striking difference between the two systems is the increase in both the real permittivity and loss of the highly viscous matrix blend (P13/VB) and the absence of this in the low viscous system. It can be seen on the SEM micrograph of Fig. 9 (P13, 18 s^{-1}) that the dispersed phase

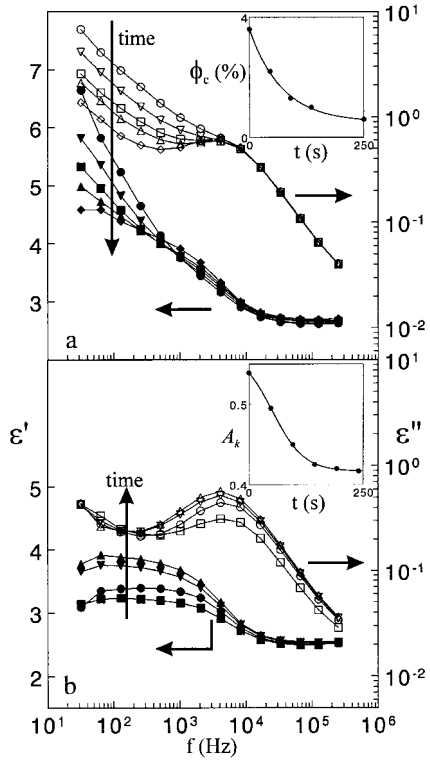

Fig. 8. Development of permittivity (●) and loss (○) of two 20 vol.% Vectra B950 – polypropylene blends with time after cessation of flow. (a) P 13E10 and (b) PLZ 746. The inset in (a) shows the change in the volume fraction of co-continuous Vectra B950 with time. The inset in (b) depicts the change in the shape factor with time.

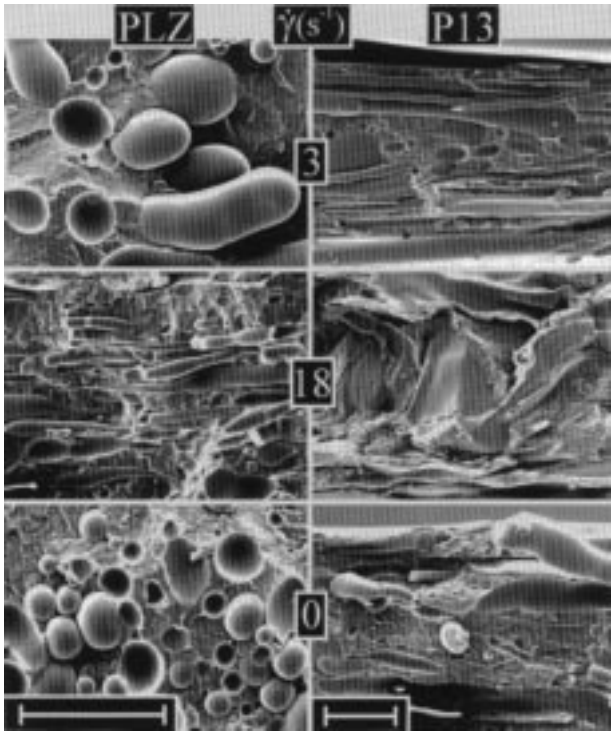

Fig. 9. SEM micrographs of two 20 vol.% Vectra B950-polypropylene blends of Fig. 8 at different shear rates: low ($3\ s^{-1}$), high ($18\ s^{-1}$) and after cessation of flow ($0\ s^{-1}$). The length of the bars in 200 μm.

in P13/VB at high shear rates is present as sheets near the outer region of the film. The sheets even penetrate into the bulk of the blend. Therefore it is possible that a structure exists which is co-continuous throughout the blend and causes percolation in the system. As the conductivity of the disperse phase is much larger than that of the matrix, this co-continuous structure will cause an increase in the overall conductivity and will induce electrode polarization in the continuous part of the Vectra phase. If we assume a simple parallel model, which gives by the way the lowest bound, we find that this continuous fraction (ϕ_c = volume fraction of Vectra B950 which is continuous, see inset Fig. 8(a)) decreases from ca. 3.6 to 0.6% after cessation of flow. In Fig. 9 (P13, $0\ s^{-1}$) it is clearly visible that the lamellar structure breaks up after cessation of polymer flow. The sheets retract or breakup into fibres and spheroids. The bi-continuous structure and percolation therefore disappears, as can be seen in Fig. 8(a). More sophisticated theories about percolation in conductor-insulator systems are given by e.g. McLachlan [28], Michels et al. [29]. and Sonneveld et al. [30].

The dispersed phase is present in the PLZ/VB system as spheroids and separate fibres (Fig. 9, PLZ, $18\ s^{-1}$). Therefore a co-continuous structure will not be formed during extrusion and no electrode polarization will occur, as can be seen in Fig. 8(b). After cessation of flow an increase in the relaxation strength can be observed. This change can be converted to values of the shape factor, A_k (assuming $\beta_0' = 1$). The sizes of the particles in Fig. 9 ($r > 20$ μm and $1/\kappa = 0.5$ μm $\rightarrow \beta_0' > 0.98$) justify the use of $\beta_0' = 1$ in Eq. (2). The evaluation of the shape factor calculated using Eq. (1) is shown in the inset of Fig. 8(b). It is clear that the *L/D* of the fibres decreases (A_k changes from 0.53 to 0.4) and thus the fibres retract or breakup into spheres. SEM micrographs of the system before and after breakup show this difference (Fig. 9 PLZ, $18\ s^{-1}$ and PLZ, $0\ s^{-1}$). This illustrates that it is possible to follow the breakup of the morphology in time using dielectric spectroscopy.

4.6. During polymer flow

More difficult to analyze are the dielectric results during polymer flow. This is caused by the uncertainty of the electrode spacing. In this section we will use the data of Fig. 3 and Eq. (5) to correct for the change in electrode spacing.

4.7. Formation of morphology

In the previous section we studied the breakup of the morphology after cessation of flow. Now we will address the formation of morphologies during the polymer flow. Fig. 10 shows the dielectric response of a high (10a) and a low viscous (10b) 20% Vectra-polypropylene blend (the same systems as in Fig. 8) for various extruder speeds and

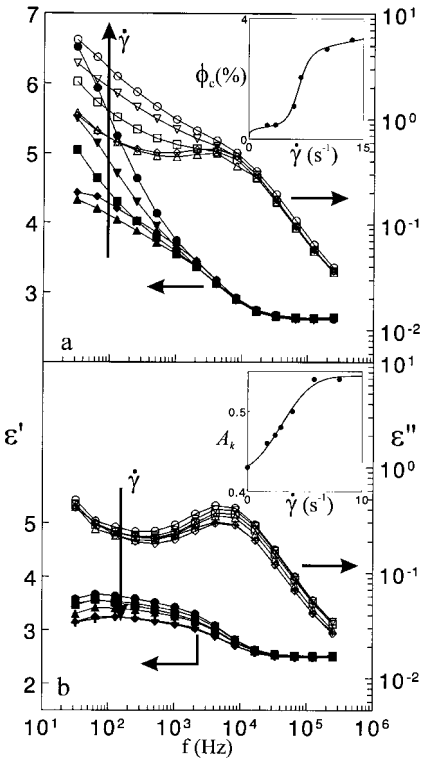

Fig. 10. Development of permittivity (●) and loss (○) of two 20 vol.% Vectra B950-polypropylene blends for increasing shear rates. (a) P 13E10 and (b) PLZ 746. The inset in (a) shows the change in the volume fraction of co-continuous Vectra B950 with increasing shear rate. The inset in (b) shows the change in the shape factor with increasing shear rate.

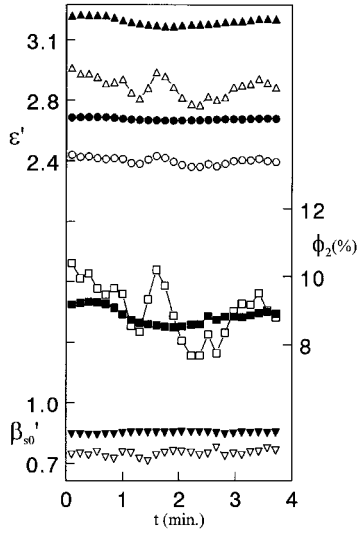

Fig. 11. Real permittivity, volume fraction of the Vectra B950 phase and size factor of a 10 vol.% Vectra B950-PS N5000 blend versus time at two different shear rates: $\langle\dot{\gamma}\rangle = 3\ s^{-1}$ (▲ = ε' (256 Hz), ● = ε' (66 kHz), ■ = ϕ_2 and ▼β_0') and $\langle\dot{\gamma}\rangle = 25\ s^{-1}$ (△ = ε' (256 Hz), ○ = ε' (66 kHz), □ = ϕ_2 and ▽ = β_0').

therefore different shear rates. An average of five frequency scans was taken at each shear rate. The graphs in Fig. 10 are similar to those in Fig. 8. We can therefore conclude that the formation of the morphology in the two systems is the reverse of the breakup: a higher shear rate causes fibres to form inside the mixing section. For the P13 matrix, both fibres and spheres are formed (Fig. 9, P13, 3 s^{-1}) at low shear rates. The higher the shear rate the more electrode polarization occurs and therefore a higher continuous fraction is formed (Fig. 9, P13, 18 s^{-1}). The calculated values of this continuous fraction versus shear rate are shown in the inset of Fig. 10(a). At the lowest shear rate about 0.5% of the Vectra phase is continuous, whereas at the highest shear rate this fraction is more than 3%. So, dielectric spectroscopy is a suitable technique for the research on co-continuous morphologies. The conduction and electrode polarization in the blend is an indication for the presence of a co-continuous morphology.

The graphs of dielectric response for the low viscous matrix (Fig. 10(b)) do not show the formation of a continuous fraction. The magnitude of the relaxation strength decreases with increasing shear rate. This indicates the formation of more elongated particles during flow ($\Delta\varepsilon \downarrow \leftrightarrow A_k \uparrow$). The calculated values of the shape factor versus the shear rate are depicted in the inset of fig. 10(b). As the particles are rather large (>20 μm), even at the highest shear rate, the value of β_0' is kept at 1. It is clearly visible that a more fibrous structure is formed at high shear rates (A_k changes from 0.43 to 0.54). This is corroborated by the SEM micrographs in Fig. 9: low shear rate in Fig. 9, PLZ, 3 s^{-1} and high shear rate in Fig. 9, PLZ, 18 s^{-1}.

4.8. Time dependent measurements

Up to now we did not address the possible errors involved in the calculations. In order to obtain information about this uncertainty, we monitored the dielectric response at two frequencies for a period of time. In Fig. 11 the real permittivity of a 10% Vectra/PS5 blend at 256 Hz and 66 kHz is given for two shear rates: 3 and 25 s^{-1} (average pressures 29 and 133 bar respectively). The values at the high frequency fluctuate less than those at the low frequency for both shear rates. Furthermore, the permittivities at the low shear rate show smoother graphs versus time. This is caused by changes in the pressure in the mixing section and therefore between the electrodes. During the measuring period (4 min.), the pressure at $\langle\gamma\rangle \approx 3s^{-1}$ fluctuated between 28 and 30 bar. For $\langle\gamma\rangle \approx 25\ s^{-1}$ this pressure varied between 128 and 138 bar. At higher extruder speed this range becomes even broader. As we use an average pressure and thus an average correction parameter, d_c, for the calculations, the error at higher shear rates will increase, as can be seen in Fig. 11 by comparing the $\beta_0'$and ϕ_2 values at the two shear rates. In appendix B, we will present an alternative data processing, which includes the loss data in the calculations. This is somewhat more elaborate and requires

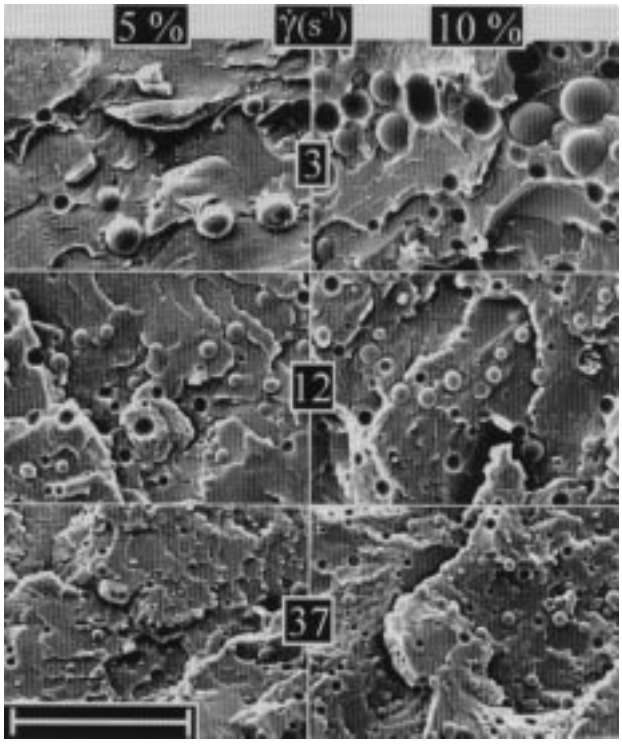

Fig. 12. SEM micrographs of two Vectra B950-polystyrene blends for the volume fractions Vectra B950 of 5 and 10% at low (3 s^{-1}), medium (12 s^{-1}) and high shear rates (37 s^{-1}). The length of the bar is 100 μm.

reliable values for the dielectric loss of both the Vectra and the blends. Admittedly a small change in the conductivity of the materials can have a large influence on the outcome of the calculations, so that the improvement in reliability might be small. Therefore, we have preferred to use the method with known d_c in this article.

4.9. Particle size

SEM analysis of the 5 and 10% blend of Vectra and the highly viscous polystyrene PS5 shows that the dispersed phase is present as spheres for all shear rates studied (Fig. 12). This means that the value of the shape factor A_k can be kept constant at 1/3. Knowing this value, the particle size can be studied, via the parameter β'_{s0}. The development of the real permittivity was monitored for 4 min. at frequencies above (66 kHz) and below (256 Hz) the interfacial relaxation peak. The average pressure was used to estimate the value of d_c. The calculated values for $\beta_{s0}{}'$ are plotted in Fig. 13 together with the error bars. On the right *y*-axis the particle size is indicated. This size was calculated from $\beta_{s0}{}'$ ($\omega = 0$, Eq. (2)) and assuming a Debye length ($1/\kappa$) of approximately 0.5 μm. When comparing the absolute particle size obtained from the SEM micrographs in Fig. 12 to the curves in Fig. 13, we find a very good agreement for the 5% blend (the results are listed in table 2). However, the agreement between the dielectric and SEM results for the 10% blend is less satisfactory.

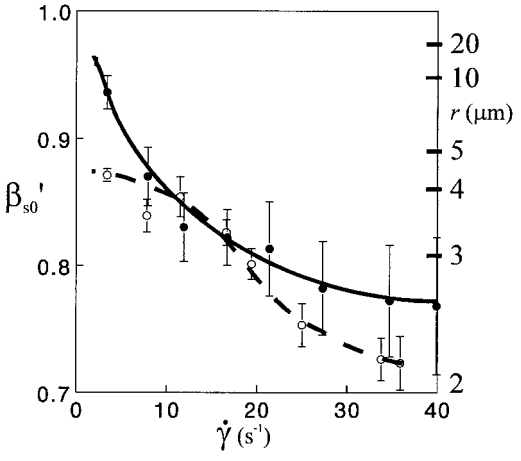

Fig. 13. Development of the size factor and particle diameter with increasing shear rate for a 5 vol.% (–●–) and 10 vol.% (–○–) Vectra B950 blend in polystyrene N5000.

Table 2
Particle sizes obtained using dielectric spectroscopy and SEM analysis for the 5 vol.% blend of Vectra B950 in polystyrene N5000. The sizes were calculated from the β'_0 parameters using a Debye length of 0.5 μm in Eq. (2)

$\langle\dot{\gamma}\rangle$ (s^{-1})	β'_0	r (μm) (diel)	r (μm) (SEM)
3	0.94	8.8	9 ± 3
8	0.87	4.3	5.6 ± 2.0
12	0.83	3.3	4.2 ± 1.6
27	0.78	2.7	2.8 ± 0.9
40	0.76	2.5	2.5 ± 0.9

Clearly, the size of the particles decreases with increasing shear rate for both volume fractions. This was also demonstrated by the SEM micrographs in Fig. 12 and the dielectric experiments in Fig. 13. This proves that on-line dielectric spectroscopy can be used to compare the particle sizes during extrusion of polymer blends. It was not possible to compare the results of the two blends, since we do not exactly know the validity of the generalized Böttcher–Trukhan model with increasing volume fraction of the inclusions. It is also possible that the relation between the pressure and the electrode spacing changes as the volume fraction increases, as a result of a change in the rheological properties of the blends. It is therefore highly recommended for future work, that the sheet extrusion die is stiff enough to withstand the pressures, or contains an electrode system, which cannot be deformed.

As predicted in the previous section, the size of the error bars increases with increasing shear rate. This is more pronounced for the 5% blend. The reason for this is that the absolute value of the relaxation strength is smaller for the 5% blend, thus the signal–noise ratio is worse.

5. Conclusions

Dielectric spectroscopy turns out to be a useful technique

for on-line characterization of the morphology of polymer blends. Admittedly, in the present setup, the spacing of the electrodes increased with increasing internal pressure in the extruder. Nevertheless, it was possible to convert the measured dielectric data into reliable values of the parameters describing the shape and size of the dispersed phase. The morphologies predicted on the basis of the dielectric data were confirmed by SEM micrographs.

The evolution of the shape factor with shear rate and time (after cessation of flow) was assessed for blends of Vectra B950 and low viscous polypropylene. It was found that with increasing shear rate the dispersed phase becomes more fibrous. The formation of a co-continuous morphology at an increasing shear rate and subsequently breakup at a decreasing shear rate was observed for a blend of Vectra B950 and a high viscous polypropylene.

The decrease in the size of the particles with increasing shear rate was studied using blends of Vectra B950 and polystyrene (low and high viscous). At low volume fractions of the dispersed phase the calculated particle size agreed well with the one obtained from SEM.

Acknowledgements

This work was sponsored by the Netherlands Organization of Scientific Research (SON/STW-NWO).

Appendix A. The generalized Böttcher–Trukhan mixture equation

In the previous article [22], we derived the Böttcher–Trukhan for partially conducting spherical particles in an insulating matrix from the original Böttcher equation:

$$\varepsilon = \varepsilon_1 + 3\varepsilon\phi_2 \frac{\varepsilon_2 - \varepsilon_1}{\varepsilon_2 + 2\varepsilon} \tag{A.1}$$

We also indicated that the effects of both the conductivity and diffusion in the second phase are introduced in the equation by scaling the permittivity of this phase with $(1 - \beta_s^*)$ and found:

$$\varepsilon^* = \varepsilon_1 + 3\varepsilon^*\phi_2 \frac{\varepsilon_2/(1 - \beta_s^*) - \varepsilon_1}{\varepsilon_2/(1 - \beta_s^*) + 2\varepsilon^*} \tag{A.2}$$

Starting from the Böttcher–Hsu equation:

$$\varepsilon^* = \varepsilon_1 + \varepsilon^*\phi_2 \frac{\varepsilon_2 - \varepsilon_1}{\varepsilon_2 A_k + \varepsilon^*(1 - A_k)} \tag{A.3}$$

and assuming the same scaling of the permittivity of the ion containing phase, albeit now with $(1 - \beta^*)$, rather than β_s^* – in order to account for non spherical particles – we obtain:

$$\varepsilon^* = \varepsilon_1 + \varepsilon^*\phi_2 \frac{\varepsilon_2/(1 - \beta^*) - \varepsilon_1}{\varepsilon_2 A_k/(1 - \beta^*) + \varepsilon^*(1 - A_k)} \tag{A.4}$$

Appendix B. Calculation of morphology parameters using alternative data handling

In this article we have processed the data using the correction measurements of the pure matrix polymers. The average value of correction parameter, d_c, obtained from Fig. 3, was taken for the calculations. During extrusion of the blends the pressure changed, sometimes even by 20 bars. This affected the electrode spacing. It would be desirable to determine the actual value of d_c, for every frequency scan, instead of doing the correction afterwards. This is possible by invoking the dielectric loss in the calculations. An estimation for the dielectric loss at high frequencies can be derived from Eq. (1):

$$\varepsilon''_\infty \approx \beta''_\infty \varepsilon_2 \frac{\varepsilon'_\infty(\phi_2 - A_k) + \varepsilon_1 A_k}{\varepsilon_2(A_k - \phi_2) - \varepsilon_1(1 - A_k - \phi_2) + 2\varepsilon'_\infty(1 - A_k)} \tag{B.1}$$

β''_∞ is the imaginary part of β^* at high frequencies and is equal to $1/(\omega\tau_2) = \varepsilon''_2/\varepsilon'_2$. From Eq. (B.1) for the loss at high frequencies and Eq. ($1'$) for both low (β'_0) and high ($\beta'_\infty = 0$) frequencies, we can obtain three equations:

$$A_k[\varepsilon'_\infty(\varepsilon_2 + \varepsilon_1 - 2\varepsilon'_\infty) - \beta''_\infty\varepsilon_2(\varepsilon_1 - \varepsilon'_\infty)] + \phi_2[\varepsilon''_\infty(\varepsilon_1 - \varepsilon_2) - \beta''_\infty\varepsilon_2\varepsilon'_\infty] = \varepsilon''_\infty[2\varepsilon'_\infty - \varepsilon_1] \tag{B.2}$$

$$A_k(\varepsilon'_s - \varepsilon_1)(\varepsilon'_s - \varepsilon_2)/(1 - \beta'_0) - \phi_2\varepsilon'_s(\varepsilon_1 - \varepsilon_2)/(1 - \beta'_0) = \varepsilon'_s(\varepsilon'_s - \varepsilon_1) \tag{B.3}$$

$$A_k(\varepsilon'_\infty - \varepsilon_1)(\varepsilon'_\infty - \varepsilon_2) - \phi_2\varepsilon'_\infty(\varepsilon_1 - \varepsilon_2) = \varepsilon'_\infty(\varepsilon'_\infty - \varepsilon_1) \tag{B.4}$$

We will also take the corrected values of the loss and permittivity:

$$\varepsilon''_m = \varepsilon'' d_c \quad \text{and} \quad \varepsilon'_m = \varepsilon' d_c \tag{B.5}$$

Eqs. (B.2)–(B.5) make it possible to calculate with linear least squares the three unknown parameters: viz. the volume fraction of the dispersed phase, ϕ_2, the correction factor, d_c and the size parameter, β'_0.

We have compared the two data processing methods using the 5% VB/PS5 blend at a shear rate of 17 s^{-1}. The measured real permittivity at 256 and 66 kHz and the loss at 66 kHz versus time are plotted in Fig. 14. The calculated values of β'_0 for both methods are also given. It is clear that the two calculation methods do not differ much. The average values of β'_0 are also comparable: 0.839 ± 0.023 when d_c is known and 0.816 ± 0.021 when d_c is calculated. The error is slightly less for the latter method. As the more elaborate method hardly gives much better results, we used the simpler method for our calculations in this article.

The volume fraction of dispersed phase was also determined by both methods. It was found that the average values

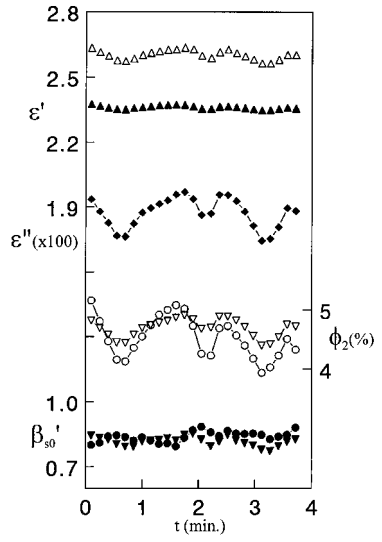

Fig. 14. Real permittivity (▲ = ε' (256 Hz), △ = ε' (66 Hz)), loss (◆ = ε'' (66 kHz) × 100), volume fraction of the Vectra B950 phase and size factor of a 5 vol.% Vectra B950-PS N5000 blend versus time at a shear rate of 17 s^{-1}. Comparison of the two data processing methods: ϕ_2 = ○ and β_0' = ● for known d_c and ϕ_2 = ▽ and β_0' = ▼ for calculated d_c.

were also comparable; both provide about 4.6 vol.%. The variation however, was twice as large for the method with known d_c (0.35 and 0.16 vol.% respectively). Thus the somewhat more laborious method produces a more accurate value of the volume fraction.

References

[1] Patel SH, Todd DB, Xanthos M. Annual Techn Conf Soc Plast Eng 1994;2:2214–2219.
[2] Jones RW, McClelland JF. Process Control Qual 1993;4:253–260.
[3] Morrow V. Annual Techn Conf Soc Plast Eng 1995;1:1152–1156.
[4] De Laney DE, Morrow V, Greene J. Annual Techn Conf Soc Plast Eng 1996;1:1095–1099.
[5] Gendron R, Daigneault LE, Caron L-M. Annual Techn Conf Soc Plast Eng 1996;1:1118–1122.
[6] Todd DB, Gogos CG, Esseghir M, Yu D-W, Widagdo S. Plast Eng 1997;53(3):107–108.
[7] Yu D-W, Esseghir M, Gogos CG. Annual Techn Conf Soc Plast Eng 1995;1:136–140.
[8] Cielo P. Opt Eng 1993;32(9):2130–2137.
[9] Piché L, Lévesque D, Gendron R, Tatibouët J. Annual Techn Conf Soc Plast Eng 1995;2:2715–2719.
[10] Tanzer CI, Roy AK. Annual Techn Conf Soc Plast Eng 1995;2:2700–2706.
[11] Hisao BS, Barton Jr R, Quintana J. J Appl Polym Sci 1996;62:2061–2068.
[12] Siano SA. Biotechnol Bioeng 1997;55(2):289–304.
[13] Hilland J. Meas Sci Technol 1995;8:901–910.
[14] Perl JP, Thomas C, Wasan DT. J Colloid Interface Sci 1990;137(2):425–432.
[15] King RJ, King KV, IEEF Instr Meas Techn Conf IEEE Piscataway, 1991, 506–512.
[16] King RJ. Appl Eng Agr 1997;13(3):361–371.
[17] Golba Jr JC, Shete PK, U.S. Patent 4 448 909, 1984.
[18] Golba Jr JC, Hansen MG, U.S. Patent 4 448 943, 1984.
[19] McBrearty M, Perusich SA, U.S. Patent 5 208 544, 1993.
[20] Boersma A, Wübbenhorst M, van Turnhout J. Macromolecules 1997;30(10):2915–2922.
[21] Boersma A, van Turnhout J. J Polym Sci, Polym Phys Ed 1998;36:815–825.
[22] Boersma A, van Turnhout J. J Polym Sci, Polym Phys Ed 1998;36:2835–2848.
[23] Roetting O, Hinrichsen G. J Thermoplast Comp Mater 1995;8:252–259.
[24] Roetting O, Hinrichsen G. J Thermoplast Comp Mater 1997;10:524–531.
[25] Trukhan EM. Soviet Phys Solid State 1963;4(12):2560–2570.
[26] Dukhin SS, Shilov VN, Dielectric phenomena and the double layer in disperse systems and polyelectrolytes. New York: Wiley, 1974, p. 32–37.
[27] Malmgren-Hansen B, Sørensen TS, Jensen JB, Henneberg M. J Colloid Interface Sci 1989;130(2):359–385.
[28] McLachlan DS. J Phys C: Solid State Phys 1987;20:865–877.
[29] Michels MAJ, Brokken-Zijp JCM. Ned Tijdschr Natuurkd 1989;A55(3):93–97.
[30] Sonneveld PJ, Visscher W, Panneflek F, Barendrecht E, Michels MAJ. J Appl Electrochem 1992;22:935–949.